Two-step co-sintering method to fabricate anode-supported Ba₃Ca₁.₁₈Nb₁.₈₂O₉₋δ proton-conducting solid oxide fuel cells

Siwei Wang [a], Lei Zhang [a], Zhibin Yang [a], Lingling Zhang [a], Shumin Fang [a], Kyle Brinkman [b], Fanglin Chen [a],[*]

[a] Department of Mechanical Engineering, University of South Carolina, Columbia, SC 29208, USA
[b] Savannah River National Laboratory, Aiken, SC 29808, USA

HIGHLIGHTS

► Ba₃Ca₁.₁₈Nb₁.₈₂O₉₋δ (BCN18)-based SOFCs were fabricated by novel two-step co-sintering method.
► Low co-sintering temperature was achieved for anode-supported SOFCs using BCN18 electrolyte.
► Dense BCN18 electrolyte and porous anode with fine particles were obtained.
► Combined with proper electrodes, two-step co-sintering led to higher cell performance.

ARTICLE INFO

ABSTRACT

Anode-supported solid oxide fuel cells (SOFCs) based on complex-perovskite structured Ba₃Ca₁.₁₈Nb₁.₈₂O₉₋δ (BCN18) proton-conducting electrolyte membranes have been successfully fabricated by a novel two-step co-sintering method. BCN18 has been reported to have excellent chemical stability against H_2O and CO_2, but is relatively difficult to densify. In this study, dense BCN18 electrolyte membranes with fine grain size have been obtained by a novel two-step co-sintering method at a relatively low sintering temperature of 1,300 °C, compared to the typical high sintering temperature of 1,550 °C. Furthermore, the Ni–BaZr₀.₁Ce₀.₇Y₀.₁Yb₀.₁O₃₋δ anode obtained by the novel two-step co-sintering method was composed of small particles with high porosity which is advantageous for electrode performance. Single fuel cells using BCN18 as the electrolyte, Ni–BaZr₀.₁Ce₀.₇Y₀.₁Yb₀.₁O₃₋δ as anode and Ba₀.₉Co₀.₇Fe₀.₂Nb₀.₁O₃₋δ as cathode demonstrated a power density of 106 mW cm⁻² at 750 °C, the best fuel cell performance ever reported for the BCN18 electrolyte. These results suggest that the two-step co-sintering method is a promising method to optimize the microstructure, and combined with proper electrodes, enhanced performance of anode-supported SOFCs using BCN18 proton-conducting electrolyte can be obtained.

1. Introduction

Proton-conducting solid oxide fuel cells (PC-SOFCs) have the unique property of conducting protons from the anode (hydrogen electrode) to the cathode (oxygen electrode), while producing water at the cathode side which avoids fuel dilution problems for SOFCs as compared to conventional oxygen-ion-conducting electrolytes. Furthermore, solid oxide electrolysis cells (SOECs) using proton-conducting electrolyte can produce pure and dry hydrogen on the hydrogen electrode, a significant advantage compared with those using oxygen-ion-conducting electrolytes where hydrogen is produced concurrently with steam requiring further drying steps [1]. In addition, the lower activation energy and relatively high proton conductivity at intermediate temperatures attainable from proton conducting oxides enables reduced operating temperature PC-SOFCs, potentially lowering the cost and enhancing the durability and reliability of SOFC systems [2].

Among the different types of solid-state proton conducting materials, the most extensively studied materials are simple perovskite structured AMO₃-based proton conductors (A=Ba and/or Sr while M=Ce, Zr, Ta and In, or a solid solution of multiple elements in the B-site, doped with Y and/or lanthanides such as Yb, Gd, Nd, and Sm in the B-site [3–6]). However, it is extremely difficult to achieve both good chemical stability and high electrical

conductivity in these materials. Although $BaCeO_3$-based PC-SOFCs have demonstrated high power output, the long term stability is an issue since $BaCeO_3$ has relatively low chemical stability in water and CO_2 atmospheres at typical SOFC operating conditions. $BaZrO_3$-based proton conductors show good chemical stability but the total conductivity is relatively low [7,8]. Consequently, significant efforts have been made in exploring novel proton conducting oxides with improved chemical stability and acceptable conductivity [9–12]. Among the different novel materials explored, complex-perovskite structured $Ba_3Ca_{1.18}Nb_{1.82}O_{9-\delta}$ (BCN18) has been reported to possess acceptable conductivity and excellent chemical stability towards CO_2 and H_2O at the typical SOFC operating conditions [13,14]. In addition, it has been recently discovered that dopants in the Nb sites can improve proton conductivity without sacrificing the chemical stability [15]. Unfortunately, very few reports have explored the use of BCN18 materials in SOFC applications due to the low sinterability of the BCN18 electrolyte as well as the lack of compatible electrode materials [14,15]. A maximum power output of 48 mW cm^{-2} at 700 °C has been reported for SOFCs using BCN18 electrolyte membrane prepared by an *in-situ* method (to lower the sintering temperature to 1,400 °C) [16]. High sintering temperature may result in the evaporation of cations in the BCN18 electrolytes as well as the densification of the anode and Ni-coarsening, deteriorating the cell electrochemical performance.

The two-step sintering method has been proved to be a simple and effective approach to prepare fine-grained dense oxide materials with significantly reduced sintering temperature [17–21]. The sample is typically preheated to a higher temperature followed by rapid cooling to an intermediate temperature which is maintained constant for long durations in order to suppress grain boundary migration (which occurs at higher temperature) while still keeping active grain boundary diffusion (which occurs at lower temperature) [17]. In this study, we have applied a two-step co-sintering (denoted as TS-CS afterwards) method to fabricate SOFCs based on BCN18 electrolyte. By co-pressing the Ni-based anode and BCN18 electrolyte and then co-sintering the bi-layer with a two-step sintering method, dense BCN18 electrolyte membrane and porous Ni-based anode with fine particle sizes have been obtained at a significantly reduced co-sintering temperature of 1,300 °C $Ba_{0.9}Co_{0.7}Fe_{0.2}Nb_{0.1}O_{3-\delta}$ (BCFN) has been chosen as cathode material in this work due to its high electrochemical performance and good chemical stability [22]. The cell performance based on BCN18 electrolyte has been evaluated using humidified hydrogen as fuel and ambient air as oxidant. Significant improvement in cell performance has been achieved compared with the BCN18 proton conducting SOFCs fabricated using the conventional sintering process.

2. Experimental

Powder samples of $Ba_3Ca_{1.18}Nb_{1.82}O_{9-\delta}$ (BCN) electrolyte were prepared by conventional solid-state reaction method as reported elsewhere [15,23]. Pure BCN18 powder was finally obtained after calcination at 1,200 °C for 5 h in air with a heating rate of 3 °C min^{-1}. For fuel cell fabrication, NiO–$BaZr_{0.1}Ce_{0.7}Y_{0.1}Yb_{0.1}O_{3-\delta}$ composite was adopted as the anode and $Ba_{0.9}Co_{0.7}Fe_{0.2}Nb_{0.1}O_{3-\delta}$ was chosen as the cathode material. The former showed excellent performance as a composite anode material [4], and the latter showed good compatibility with the thermal expansion coefficient of BCN18 and good performance as a cathode [22]. Phase formation of the samples were determined by a Mini X-ray powder diffractometer (Rigaku, Japan) with graphite-monochromatized CuKa radiation ($\lambda = 1.5418$ Å) with a scanning rate of 5° min^{-1}. Morphologies were characterized by scanning electron microscopy (SEM, FEI Quanta and XL 30) and thermal field emission scanning electron microscopy

(FESEM, Zeiss Ultra plus) equipped with an energy dispersive X-ray spectroscopy (EDS) analyzer. The anode substrates containing NiO (J.T. Baker, 99%), $BaZr_{0.1}Ce_{0.7}Y_{0.1}O_{3-\delta}$ (BZCYYb) [24] and graphite (Alfa Aesar, 99.8%) with a weight ratio of 3:2:1 were fabricated by die pressing under 100 MPa. BCN18 electrolyte powder was then added onto the substrate and co-pressed at 300 MPa to form a bi-layer [25]. The green bi-layers were subsequently treated with TS-CS method using the profile shown in Fig. 1. The bi-layer was first preheated to 1,450 °C to achieve an intermediate density for the electrolyte, and then rapidly cooling down to 1,300 °C and hold for 20 h to allow full densification of the electrolyte membrane. After TS-CS treatment, dense BCN18 electrolyte film with a thickness of 25 μm on the porous NiO-BZCYYb anode substrate was obtained. The BCFN cathode ink was prepared by ball-milling with an organic solvent (V-006, Her-aeus) and subsequently pasted on the BCN18 electrolyte surface of the as-prepared electrolyte/anode bi-layer, followed by firing at 1,000 °C for 2 h to form a single cell. The thickness of the cathode was approximately 35 μm and the effective area of the cathode was 0.33 cm^2. Single cells were sealed on alumina tubes using silver paste and ceramic bond. Cells were tested with hydrogen (containing 3 vol % H_2O) as fuel and ambient air as the oxidant. The cells were stabilized at 750 °C to allow NiO fully reduced to Ni particles before the electrochemical tests. Cell power output and AC impedance spectra were measured using a Versa STAT3-400 electrochemical station with an applied 10 mV perturbation voltage.

3. Results and discussion

3.1. Sinterability

Fig. 1 shows the sintering profile and dilatometry study of the two-step sintering method applied to the BCN18 electrolyte. The sintering behavior for BCN18 using conventional sintering method has also been included for comparison. For the conventional sintering, the sample was heated at 1,450 °C and held for 5 h. While for the two-step sintering, the BCN18 material was preheated at 1,450 °C for 1 min followed by rapid cooling to 1,300 °C and then held for 20 h. Although the sample sintered using the conventional sintering method exhibits higher linear shrinkage, the temperature at which the maximum linear shrinkage rate $(dL/dt)_{max}$ appears is similar to that of the two-step sintering method. The sample sintered by the two-step sintering method exhibits larger $(dL/dt)_{max}$ as shown in the inset in Fig. 1, probably caused by the suddenly cooling down of the sample immediately after 1,450 °C. After applying TS-CS method to the anode-electrolyte bi-layer, the electrolyte membrane is
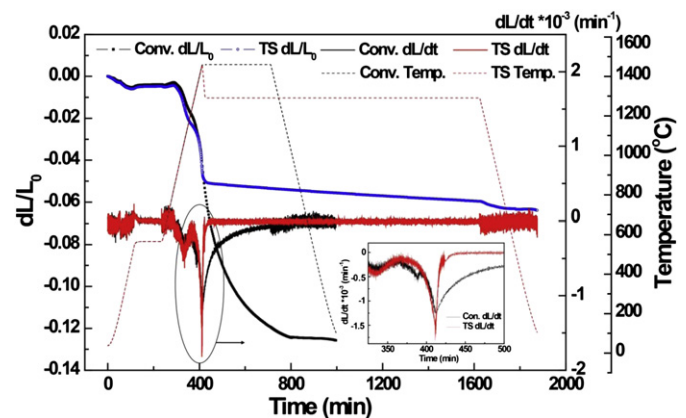

Fig. 1. Sintering profiles and dilatometric curves of BCN18 electrolyte material with conventional (Conv.) sintering and two-step (TS) sintering method, inset is expanded view of the linear shrinkage rate (dL/dt).
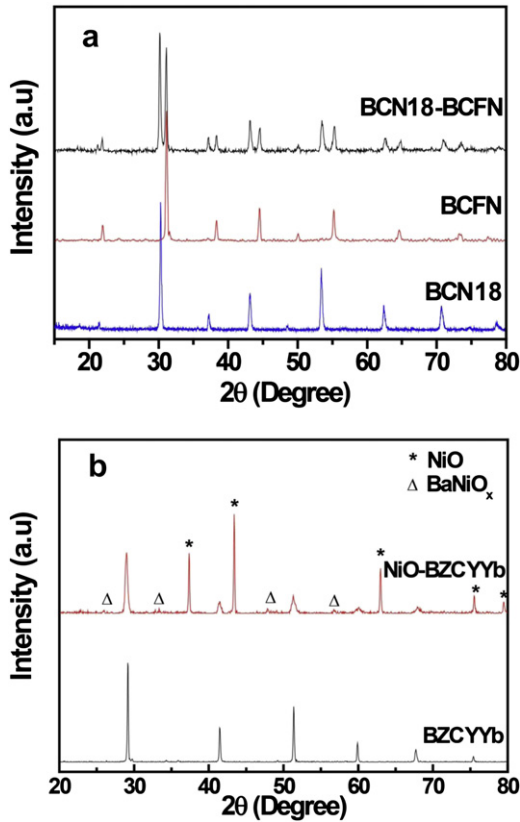
Fig. 2. XRD patterns for (a) BCN18 electrolyte, BCFN cathode and BCN18-BCFN powder mixture heated at 1,100 °C for 2 h; (b) BZCYYb, and NiO-BZCYYb powder mixture heated at 1,400 °C for 5 h.

densified (as shown in the SEM pictures in Fig. 6) with the assistance of the driven force originated from the shrinkage of the anode substrate during the co-sintering process.

3.2. Phase analysis

To check the chemical compatibility between the electrolyte and the cathode, BCN18 and BCFN with weight ratio of 1:1 were mechanically mixed and heated to 1,100 °C for 2 h. Fig. 2(a) shows the XRD patterns of BCN18 and BCFN and their mixture after heat
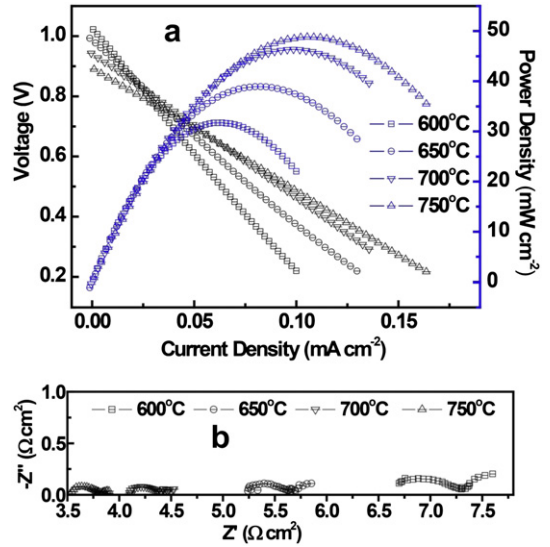

Fig. 4. (a) Cell voltage and power density as a function of current density for Ni-BCN18|BCN18|BCFN single cell fabricated by conventional sintering method at 1,400 °C for 5 h, and (b) impedance spectra of the single cell under open-circuit conditions.

treatment. No observable secondary peaks can be detected, implying that BCN18 and BCFN are chemically compatible during the fuel cell fabrication and testing processes. XRD patterns for the anode composite NiO-BZCYYb after co-sintering at 1,400 °C for 5 h exhibit predominantly NiO and BZCYYb phases, while minor peaks corresponding to $BaNiO_x$ secondary phase are found, as shown in Fig. 2(b), indicating that trace amount of BaO–NiO solid solution might be formed during the high temperature co-sintering process [26]. A NiO-BCN18 composite was not chosen as the anode since CaO in BCN18 reacts with NiO to form CaO–NiO solid solutions at the co-sintering temperatures [27,28]. In BCN18 ($Ba_3Ca_{1.18}Nb_{1.82}O_{9-\delta}$), the inclusion of extra CaO results in oxygen vacancies and thus enhanced ionic conductivity for the material [9]. The solid solution of CaO–NiO formed in the anode will thus be detrimental to the electrical conductivity of BCN18 in the anode due to the loss of CaO. The overall electrochemical performance for fuel cells with NiO-BCN18 as an anode might not be as good as the NiO-BZCYYb materials system. To confirm this, a NiO-BCN18 composite was sintered at 1,400 °C for 5 h and the back-scattered electron (BSE) image and spot scan of the EDS patterns for the grains were taken. Two phases were clearly formed as shown in Fig. 3(a). However, nickel peaks can be found from the spot
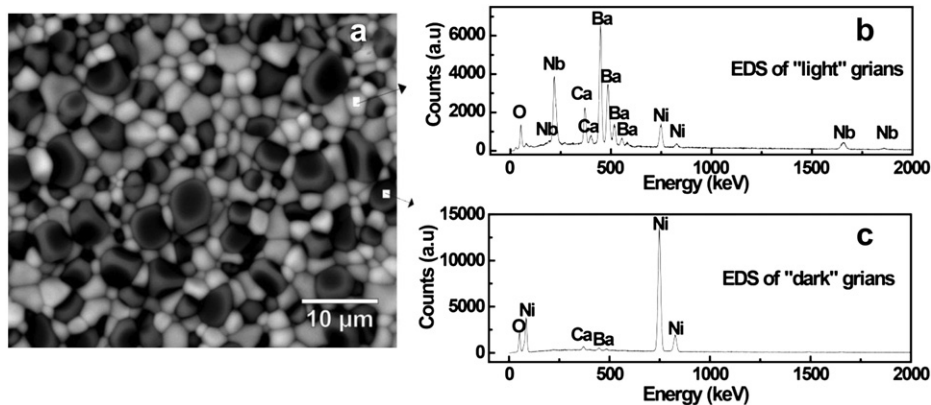

Fig. 3. (a) Back-scattered electron (BSE) image of NiO-BCN18 composite sintered at 1,400 °C for 5 h, EDS pattern of "light" grains (b) and "dark" grains (c).
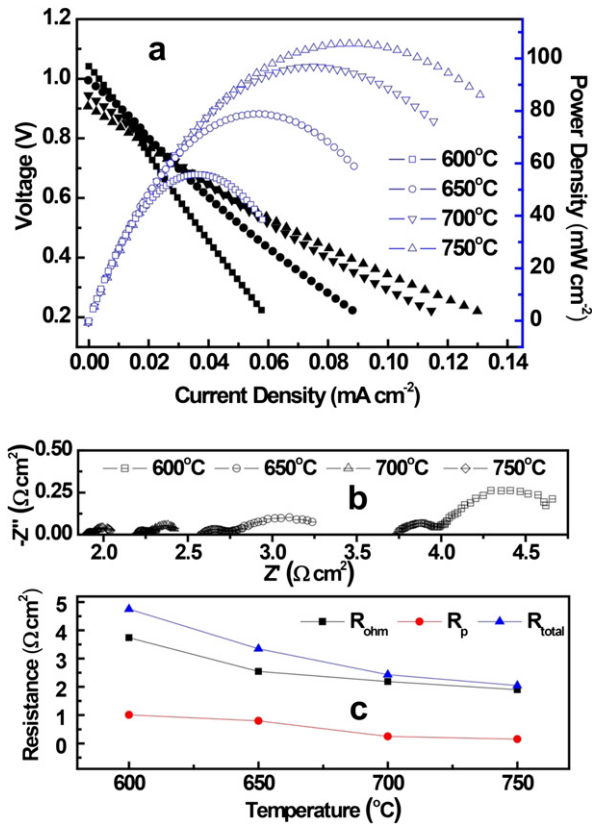
Fig. 5. (a) Cell voltage and power density as a function of current density for Ni-BZCYYb|BCN18|BCFN single cell at different temperatures, and Impedance spectra and resistances of the single cell under open-circuit conditions: (b) impedance spectra of the single cell at different temperatures, and (c) the ohmic resistance (R_{ohm}), the polarization resistance (R_p) and the total resistance (R_{total}) of the cell as a function of operating temperature.

scan of EDS patterns for the ceramics phases ("light" grains in the BSE images) as shown in Fig. 3(b), indicating that NiO dissolved into BCN18. EDS patterns for nickel phases ("dark" grains in the BSE images) shown in Fig. 3(c) also suggest that trace amount of BaO and CaO dissolved into NiO. NiO-BCN18|BCN18|BCFN fuel cells were fabricated and showed a fairly low power output of 46 mW cm^{-2} at 700 °C, similar to the reported data [16], mainly due to the relatively large ohmic resistance (shown in Fig. 4).

3.3. Electrochemical performance

Shown in Fig. 5(a) are the I−V curves and power density of the BCN18 cell fabricated by TS-CS method at different temperatures. Maximum power densities of 56, 79, 97, and 106 mW cm^{-2} with open-circuit voltage (OCV) values of 1.04, 1, 0.95 and 0.91 V were obtained at 600, 650, 700 and 750 °C, respectively. The OCV values are consistent with the reported data, indicating that the electrolyte membrane is sufficiently dense [16]. The OCV values are lower than the Nernst potentials, especially at high temperatures, which may be caused by the increased electronic conduction with temperature for the proton conducting BCN18 electrolyte membranes. With increase in the operating temperature, the electronic conductivity increases resulted through the following defect equations:

$$O_2 + 2V_O^{\cdot\cdot} \leftrightarrow 2O_O^{\times} + 2h^{\cdot} \tag{1}$$

$$H_2(g) + 2O_O^{\times} \leftrightarrow 2OH_O^{\cdot} + 2e' \tag{2}$$

where $V_O^{\cdot\cdot}$ represents oxygen vacancy, $O_O^{\times}$ represents lattice oxygen, and $OH_O^{\cdot}$ represents proton charge carrier. The electrolyte may show p-type conduction near the cathode side and n-type conduction near the anode side in the fuel cell operating conditions. The maximum power output obtained in this study is more than doubled compared with those using BCN18 electrolyte
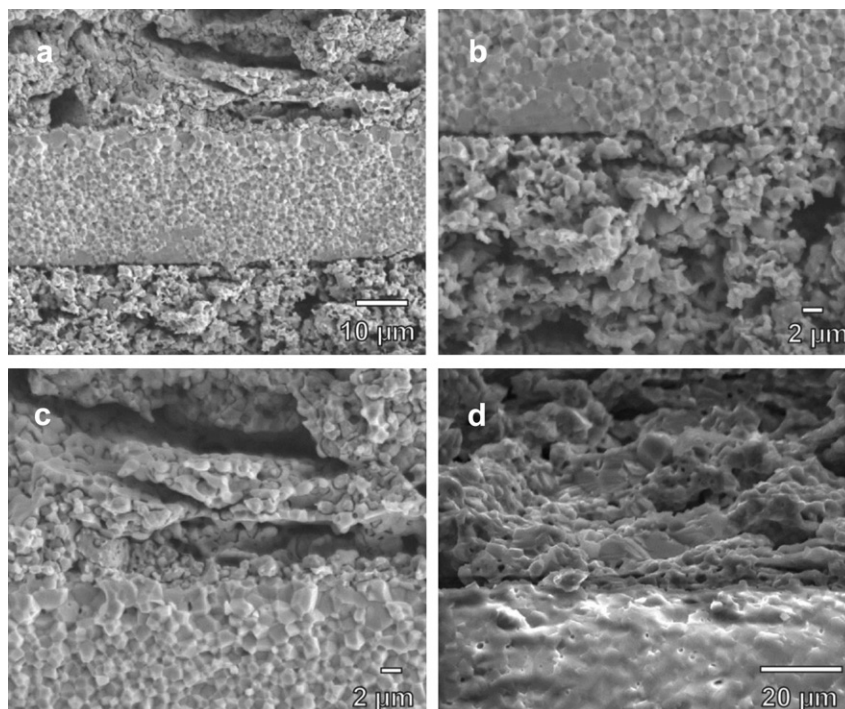

Fig. 6. Cross-sectional SEM images of post-tested Ni-BZCYYb|BCN18|BCFN SOFC fabricated by two-step co-sintering method: (a) single cell, (b) electrolyte−cathode interface, (c) electrolyte−anode interface, and (d) electrolyte−anode interface sintered by conventional sintering method.

Table 1
The ohmic resistance R_o, polarization resistance R_p and total resistance R_t obtained from the impedance spectra and their ratios.

Temperature (°C)	R_o (Ω cm^2)	R_p (Ω cm^2)	R_t (Ω cm^2)	R_o/R_t	R_p/R_t
600	3.74	1.01	4.75	78.7%	21.3%
650	2.55	0.80	3.35	76.1%	23.9%
700	2.19	0.24	2.43	89.9%	9.9%
750	1.90	0.15	2.05	92.5%	7.3%

fabricated by an *in-situ* method (48 mW cm^{-2} at 700 °C) [16]. The significantly enhanced cell performance is attributed to the adoption of the TS-CS method to lower the co-sintering temperature as well as judicious selection of the anode configuration. This processes resulted in dense, fine-grained electrolyte membranes, combined with an anode composite with small particles and high porosity, resulting in a significant reduction in the ohmic polarization resistance. Fig. 5(b) shows the electrochemical impedance spectra of the cell measured under open-circuit conditions at different testing temperatures. The high frequency intercept represents the ohmic resistance of the cell (R_o), including ionic resistance of the electrolyte and electronic resistance of the electrodes. The low frequency intercept corresponds to the total resistance (R_t) of the cell. R_t includes the R_o and the interfacial polarization resistance (R_p), which corresponds to cathode-electrolyte interfacial resistance and anode-electrolyte interfacial resistance. The R_o, R_p and R_t obtained from the impedance spectra are plotted in Fig. 5(c) and summarized in Table 1. The increase in the testing temperature resulted in a significant reduction of both the R_o and R_p, with the ratio of R_o to R_t increased from 78.7% to

92.5% (See Table 1), implying that the performance of the cell is strongly limited by the ohmic resistance. The area specific ohmic resistance (ASR) contributed from the 25 μm thick BCN18 electrolyte membrane can be estimated from the conductivity of the electrolyte ($\sigma = 2 \times 10^{-3}$ S cm^{-2} at 600 °C in air) [15]. The expected ohmic resistance from the BCN18 electrolyte membrane is 1.25 Ω cm^2 at 600 °C, while the obtained ohmic resistance of the cell is 3.74 Ω cm^2 based on the cell impedance spectra. It seems that ohmic resistance of the electrodes and contact resistance between the electrolyte and the electrode still plays significant role in the total cell ohmic resistance. Furthermore, the relatively low polarization resistance indicates that BCFN may be a suitable cathode candidate for intermediate temperature SOFCs with BCN18 proton-conducting electrolytes. Further enhancements in cell performance can be expected by preparing chemical compatible electrodes with the electrolyte or utilizing electrolyte membranes with high proton conductivity such as rare-earth element doped BCN18 [15].

3.4. Microstructural analysis

The cross-sectional images of the single cell after electrochemical measurements are shown in Fig. 6(a–c). The electrolyte–anode interface sintered by the conventional sintering method at 1,400 °C for 5 h is also shown in Fig. 6(d) for comparison. It can be seen that the electrodes are well adhered to the electrolyte membrane and there are no apparent cracks in the dense BCN18 electrolyte membrane fabricated by the TS-CS method. Compared with the conventional sintering process (Fig. 6(d)), the BCN18 electrolyte grains from the TS-CS method are much finer,
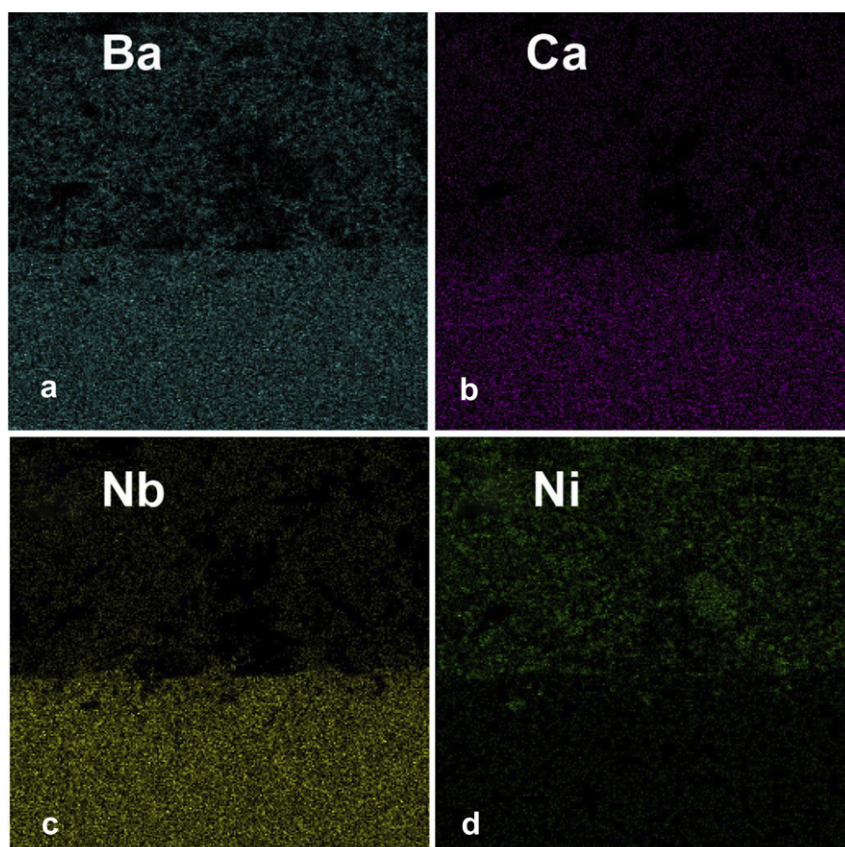

Fig. 7. EDS elemental mapping of the electrolyte–anode interface for Ni-BZCYYb|BCN18|BCFN SOFC: (a) Ba, (b) Ca, (c) Nb, (d) Ni.

characteristic of a "frozen" microstructure observed in a two-step sintering process due to the diffusion of grain boundaries without grain boundary migration [17,29]. Similar to the electrolyte, the anode particles derived from the TS-CS method are much smaller than those from the conventional sintering method. By avoiding Ni-coarsening during the sintering process, the finer anode microstructure obtainable from TS-CS method is advantageous to the cell electrochemical performance due to increased number of the triple phase boundary (TPB) sites in the anode. Selected elemental distributions from the EDS mapping of the electrolyte–anode interface are shown in Fig. 7. It can be seen that the element distributions are homogeneous in confined areas, with Ba distributed in both the anode and the electrolyte, while Ca and Nb only distributed in the electrolyte and Ni constrained only in the anode side, indicating that no observable elemental diffusions took place between the anode and the electrolyte during the fuel cell operations. It should be noted that the BCN18 electrolyte membrane fabricated by dry-pressing in the study (about 25 μm in thickness) is about 10 μm thicker than those prepared by an *in-situ* method [16]. Considering the reduced co-sintering temperature combined with 100% improvement in cell output power density, this TS-CS method has demonstrated great potential for the fabrication of anode-supported SOFCs with lower sintering temperatures and higher cell performance.

4. Conclusions

Ba$_3$Ca$_{1.18}$Nb$_{1.82}$O$_{9-\delta}$ (BCN18) proton conductor based SOFC has been successfully fabricated by a novel two-step co-sintering method. This method lowered the co-sintering temperature of the anode-electrolyte bi-layer, restricted the grain growth of the particles to obtain fine-grained dense electrolyte and ultrafine anode particles with high porosity. The BCN18 based SOFCs, combined with proper electrode materials, demonstrated the highest ever maximum power densities for these materials. The two-step co-sintering method therefore shows great potential and deserves further study for the fabrication of other anode-supported SOFC systems with optimized sintering profiles for improved electrochemical performance.

References

[1] H. Iwahara, H. Uchida, N. Maeda, J. Power Sources 7 (1982) 293–301.
[2] K.D. Kreuer, Annu. Rev. Mater. Res. 33 (2003) 333–359.
[3] J. Wu, R.A. Davies, M.S. Islam, S.M. Haile, Chem. Mater. 17 (2005) 846–851.
[4] L. Yang, S.Z. Wang, K. Blinn, M.F. Liu, Z. Liu, Z. Cheng, M.L. Liu, Science 326 (2009) 126–129.
[5] F. Chen, O.T. Søensen, G. Meng, D. Peng, Solid State Ionics 100 (1997) 63–72.
[6] M. Amsif, D. Marrero-Lopez, J.C. Ruiz-Morales, S.N. Savvin, M. Gabbás, P. Nunez, J. Power Sources 196 (2011) 3461–3469.
[7] K. Nomura, H. Kageyama, Solid State Ionics 178 (2007) 661–665.
[8] E. Fabbri, A. D'Epifanio, E. Di Bartolomeo, S. Licoccia, E. Traversa, Solid State Ionics 179 (2008) 558–564.
[9] A.S. Nowick, Y. Du, Solid State Ionics 77 (1995) 137–146.
[10] R. Haugsrud, T. Norby, Nat. Mater. 5 (2006) 193–196.
[11] E. Kendrick, J. Kendrick, K.S. Knight, M.S. Islam, P.R. Slater, Nat. Mater. 6 (2007) 871–875.
[12] J.F. Shin, L. Hussey, A. Orera, P.R. Slater, Chem. Commun. 46 (2010) 4613–4615.
[13] A.S. Nowick, Y. Du, K.C. Liang, Solid State Ionics 125 (1999) 303–311.
[14] H.G. Bohn, T. Schober, T. Mono, W. Schilling, Solid State Ionics 117 (1999) 219–228.
[15] S. Wang, F. Zhao, L. Zhang, K. Brinkman, F. Chen, J. Power Sources 196 (2011) 7917–7923.
[16] L. Bi, S.Q. Zhang, S.M. Fang, L. Zhang, H.Y. Gao, G.Y. Meng, W. Liu, J. Am. Ceram. Soc. 91 (2008) 3806–3809.
[17] I.W. Chen, X.H. Wang, Nature 404 (2000) 168–171.
[18] C.M. Lapa, D.P.F. de Souza, F.M.L. Figueiredo, F.M.B. Marques, Int. J. Hydrogen Energy 35 (2010) 2737–2741.
[19] K. Maca, V. Pouchly, P. Zalud, J. Eur. Ceram. Soc. 30 (2010) 583–589.
[20] Z. Razavi Hesabi, M. Mazaheri, T. Ebadzadeh, J. Alloys Compd. 494 (2010) 362–365.
[21] Z. Tian, X. Wang, S. Lee, K.H. Hur, L. Li, J. Am. Ceram. Soc. 94 (2011) 1119–1124.
[22] Z. Yang, C. Yang, C. Jin, M. Han, F. Chen, Electrochem. Commun. 13 (2011) 882–885.
[23] S. Wang, J. Zhai, X. Chou, L. Zhang, X. Yao, Mater. Chem. Phys. 115 (2009) 200–203.
[24] S. Wang, F. Zhao, L. Zhang, F. Chen, Solid State Ionics 213 (2012) 29–35.
[25] F. Zhao, S. Wang, L. Dixon, F. Chen, J. Power Sources 196 (2011) 7500–7504.
[26] F. Zhao, C. Jin, C. Yang, S. Wang, F. Chen, J. Power Sources 196 (2011) 688–691.
[27] D.E. Smith, T.Y. Tien, L.H. Van Vlack, J. Am. Ceram. Soc. 52 (1969) 459–460.
[28] V. Prostakova, J. Chen, E. Jak, S.A. Decterov, Calphad 37 (2012) 1–10.
[29] L. Zhang, F. Chen, C.R. Xia, Int. J. Hydrogen Energ. 35 (2010) 13262–13270.